COMBINATION OF SHAPE-CONSTRAINED AND INFLATION DEFORMABLE MODELS WITH APPLICATION TO THE SEGMENTATION OF THE LEFT ATRIAL APPENDAGE

Pol Grasland-Mongrain *

Ecole Normale Supérieure de Cachan
France

Jochen Peters, Olivier Ecabert†

Philips Research Europe–Aachen
Weisshausstr. 2, 52066 Aachen
Germany

ABSTRACT

This paper introduces a method for the flexible model-based segmentation of the whole heart from 3D CT images. The novelty of the approach is the combination in a single framework of two types of deformable models. The anatomical structures with well defined shapes (like the cardiac chambers) are segmented with deformable models constraining the deforming surface to stay close to some shape prior. On the other hand, structures with highly variable shapes are extracted by locally inflating the deforming surface without strong assumptions on the shape of the object to segment.

The proposed method has been applied to the segmentation of the heart of 17 patients. Cardiac chambers and major vessels were segmented using shape-constrained deformable models while the left atrial appendage (LAA) was extracted using the mesh inflation. Qualitatively, the mesh resulting from the inflation adapts well to the difficult shape of the LAA. However, reaching the very tip of this elongated structure remains difficult. These results are numerically confirmed with manually generated reference segmentations.

***Index Terms*—** model-based segmentation, deforming surface, mesh inflation, cardiac model, left atrial appendage

1. INTRODUCTION

The accurate segmentation of the heart, i.e., the process of assigning labels to regions in the image, is an important process in the diagnosis of cardiovascular diseases. Even if the segmentation could be done manually, it is practically impossible in daily clinical routine and much efforts have been spent on the development of semi- or fully automatic approaches.

In particular, deformable models have been widely used in the processing of cardiac images [1]. For the purpose of the chamber segmentation, shape priors showed to be useful to constraint the model deformation. A high degree of automatization could be achieved with application to computed tomography (CT) (see e.g. [2, 3]) or magnetic resonance imaging (MRI) (see e.g. [4, 5]). However, the constraints imposed by the shape prior may be too strong for substructures with highly variable shape like the left atrial appendage (LAA), which is the target structure of this work.

The LAA is a substructure of the heart above the left ventricle and connected to the left atrium (LA). It has an highly variable shape, often tubular, hooked and with a few lobes. Its size varies from 1 to 19 cm^3 [6]. It has some notable functions including the regulation of the heart function, and is involved in various heart diseases like thrombosis building, cardiac fibrillation, etc. [7].

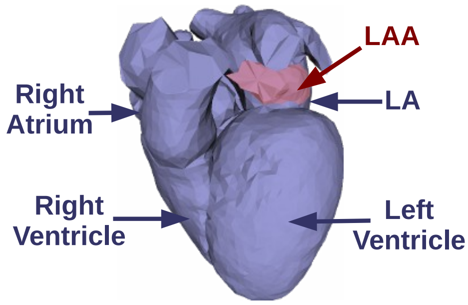

Fig. 1. Position of the LAA in the heart. Here, only the base of the LAA is highlighted, in red.

The method presented in this article builds upon a multi-step framework for the automatic segmentation of the whole heart and the major vessels in CT images introduced in [2]. Once the multi-compartment heart model is adapted to the patient's anatomy, a high resolution surface at the interface between the LA and the LAA is inflated into the LAA under the action of region forces without making explicit assumptions on the shape of the object being segmented. The novelty of the approach is that both the shape-constrained and the inflation deformable models are integrated into a single framework.

This paper is structured as follows. Section 2 briefly outlines the existing framework for whole heart segmentation [2] for completeness (first four components in Fig. 2). The new inflation algorithm (last component in Fig. 2) is described in Section 3 and evaluated in Section 4.

*pol.grasland-mongrain@ens-cachan.fr
†olivier.ecabert@philips.com

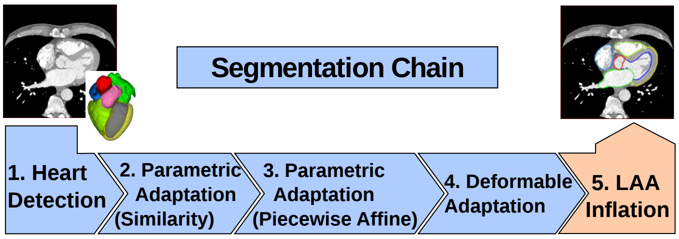

Fig. 2. Chain of modules combining the shape-constrained and inflation deformable models for heart segmentation.

2. HEART SEGMENTATION WITH SHAPE-CONSTRAINED DEFORMABLE MODELS

Automatic whole heart segmentation of the chambers is achieved in several phases which are briefly summarized below. More details can be found in [2].

Heart Detection – In the first phase, a modified Generalized Hough Transform is used to roughly localize the heart in the images and adapt the size of the model [2].

Parametric Adaptation – The second and the third phase adapt the model to the image by optimizing the parameters of a parametric transformation. In phase 2 pose misalignment is compensated by a similarity transformation, while in phase 3 a multi-affine transformation $\mathcal{T}[.]$ is optimized where each of the anatomical regions (left and right ventricles, left and right atria, and trunk of the great arteries) is assigned an affine transformation.

Practically, this adaptation is performed iterating two steps until the mesh reaches some steady state. In the first step, candidate points are detected in the image maximizing a boundary detection function, which is evaluated for each triangle along its normal vector. The point with the highest response is kept as the target point $\boldsymbol{x}_i^{\text{target}}$.

In the second step, the parametric transformations are optimized by minimizing an external energy. In this energy, the triangle centers are attracted towards target points. This target point can move without penality on the tangent plane of the surface.

Deformable Adaptation – In the fourth phase, each vertex $\boldsymbol{v}_i$ is allowed to move freely and the mesh adaptation is performed minimizing an energy function made of two contributions. The external energy introduced above is still used to attract the model towards the image boundaries while the vertex displacements are constrained by an internal energy which penalizes deviations of the deforming model from the reference shape

$$E = \alpha \cdot E_{\text{external}} + E_{\text{internal}}, \quad (1)$$

with α a weighting factor, and

$$E_{\text{internal}} = \sum_{i=1}^{V} \sum_{j \in N(i)} \left((\boldsymbol{v}_i - \boldsymbol{v}_j) - (\mathcal{T}[\boldsymbol{m}_i] - \mathcal{T}[\boldsymbol{m}_j]) \right)^2, \quad (2)$$

with $N(i)$ the set of indices of the neighbor vertices of vertex $\boldsymbol{v}_i$, and $\boldsymbol{m}_i$ the vertex coordinates of the reference model undergoing the multi-affine transformation $\mathcal{T}[.]$.

As in the previous section, mesh adaptation is performed by iterating the boundary detection step and the minimization of the Eq. (1) until a steady is state is reached.

3. LEFT ATRIAL APPENDAGE SEGMENTATION WITH INFLATION DEFORMABLE MODEL

After the model is adapted using the method described in the previous section, the position of the LA–LAA interface is known, and the surrounding substructures (LA, left ventricular myocardium, aorta, etc.) are already segmented. These two properties can be efficiently used to subsequently grow the mesh surface into the LAA.

For that purpose, the mesh at the LA–LAA interface is triangulated with high resolution to ensure reasonable triangle size when the mesh is inflated. As for the chamber segmentation, the surface is deformed by minimizing an energy function (1) where the external energy inflates the mesh and the internal energy imposes geometric regularity constraints.

3.1. Region-Based External Energy

We call the inflation external energy *region-based* energy since it makes use of the voxel gray values (Houndsfield Units) as compared to external energy from [2] which uses image edges. This region-based external energy has two components. First, it has to decide whether the mesh has to inflate or to shrink. Here, we compare the local gray value at the triangle center with a threshold differentiating between blood pool and background. Then, a target point is determined inside or outside depending on the previous comparison.

Threshold Computation – The threshold between blood pool and background is computed once before inflation and determined using the results of the previous segmentation. To find this threshold, we compute the histograms of two tissue classes from the already segmented image: the LA and the myocardium. The LAA is rather bright and has almost the same gray value as the LA, while the background is as bright as or darker than the myocardium. The optimal threshold between these two classes can be then computed by minimizing the overall voxel classification error.

Region-Based Target Point – Then, a target point $\boldsymbol{x}_i^{\text{target}}$ is computed for each triangle center $\boldsymbol{c}_i$ along its normal vector $\boldsymbol{n}_i$. This target point depends on the gray value at the location of the triangle center. If this gray value is

1. above the threshold, $\boldsymbol{c}_i$ is supposed *inside* the LAA, and $\boldsymbol{x}_i^{\text{target}}$ is set along the normal $\boldsymbol{n}_i$ pointing *outside*;

2. under the threshold, $\boldsymbol{c}_i$ is supposed *outside* the LAA, and $\boldsymbol{x}_i^{\text{target}}$ is set along the normal $\boldsymbol{n}_i$ pointing *inside*;

3. almost equal to the threshold, c_i is supposed *on the boundary*, and $\boldsymbol{x}_i^{\text{target}}$ is set at the same place as $\boldsymbol{c}_i$.

In the first two cases, $\boldsymbol{x}_i^{\text{target}}$ is successively set at a distance of 1, then 2, and finally 3 mm from $\boldsymbol{c}_i$, if at each of these positions, the point does not belong to an already segmented structure and is not on the other side of the threshold.

Region-Based External Energy – The region-based external energy can then be expressed as follows:

$$E_{\text{external, region-based}} = \sum_{i=1}^{T} \left(\boldsymbol{n}_i \cdot (\boldsymbol{x}_i^{\text{target}} - \boldsymbol{c}_i) \right)^2 \qquad (3)$$

3.2. Mesh Reference Internal Energy

The internal energy used to preserve a regular triangle distribution during inflation is the same as in Eq. (2) but instead of comparing the deforming mesh to a fixed reference shape, we use the deforming mesh at the previous iteration as reference. We can thus preserve some regular triangle distribution without making any specific assumption on the shape to be segmented.

3.3. Loop Repair During Growing

During inflation, some loops may appear. We consequently use an algorithm to detect self-intersections as introduced in [8]. It selects the triangle neighbors until the N-th order of the intersecting triangles and repairs the deformed surface by smoothing it. Further iterations of the mesh adaptation are allowed only if the number of intersection after repairing is small enough.

Smoothing is implemented by relaxing the mesh within the selected neighborhood by applying the Mesh Reference Internal Energy above without external energy contribution. We experimentally observed that neighborhoods including triangles up to the third order were sufficient. The inflation is stopped if more than ten intersecting triangles cannot be repaired.

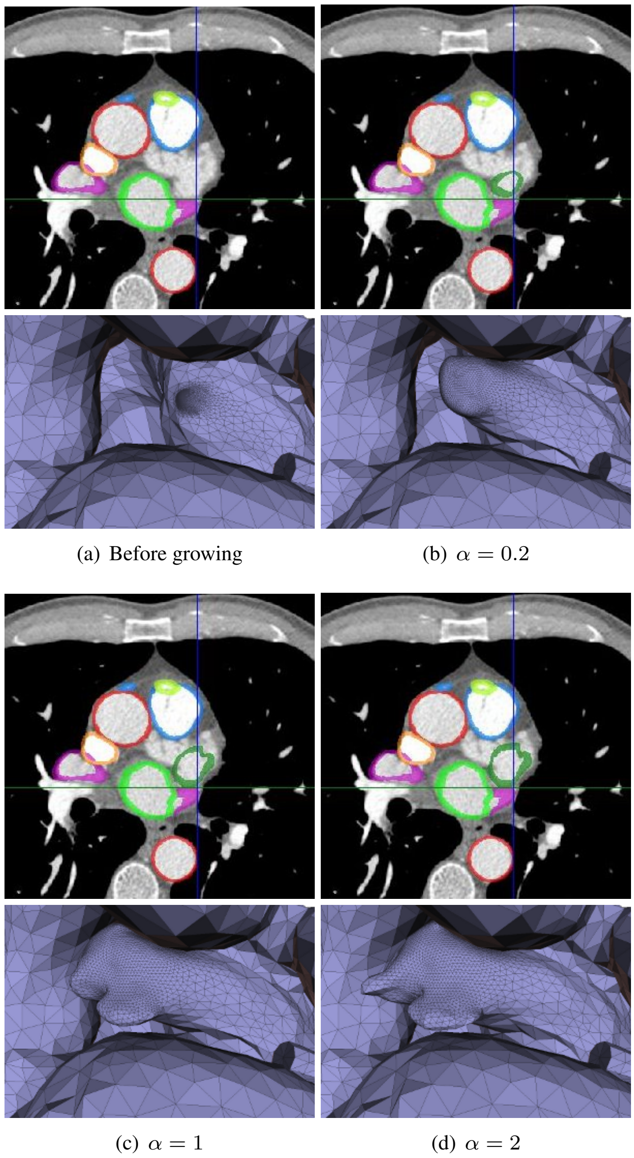

Fig. 3. Example of inflation. First picture: axial slice, from feet to head, with the substructures contours: LAA (dark green), LA (bright green), myocardium (yellow). Second picture: front view of the 3D mesh.

4. RESULTS

The algorithm takes about 50 seconds, with about 20 seconds for the LAA segmentation, on a Intel Xeon at 2,4 Ghz with 3 GB of RAM. Fig. 3 shows an example of inflation into the LAA.

In the proposed method, the weight α between the internal and external energies is successively set to 0.2, 1, 2 and 5, with each time five iterations and one loop repair. The external energy becomes thus stronger to help the mesh reach the far boundaries of the LAA. These parameters have been heuristically selected during our experiments.

A manual segmentation has been made by hand: on each 3D pictures, the four first phases of segmentation were performed. Then a operator was segmenting the LAA with a brush layer by layer. The segmentation was beginning from the base of the LAA until the borders characterized by a fixed gray value (value potentially different between different pictures). Then this LAA segmentation was slightly smoothed.

Numerical results computed by comparing manually segmented voxels (ground truth) and algorithm-segmented voxels for 17 patients are presented Fig. 4. The blue bar is the *Sensitivity*. It represents the percentage of voxels belonging to the LAA which have been segmented by the algorithm. The red bar is the *Positive Predictive Value* (PPV). It represents the percentage of voxels segmented by the algorithm which truly

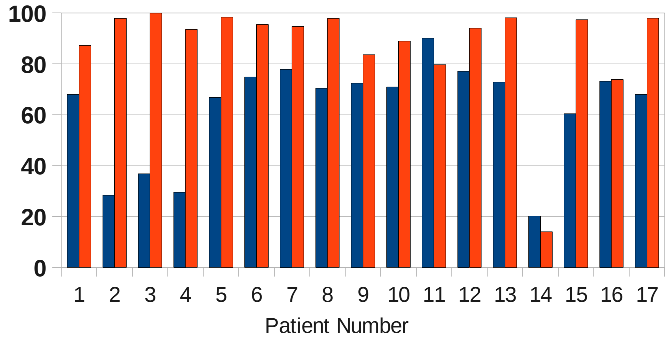

Fig. 4. Numerical evaluation of the LAA segmentation for 17 patients. The first bar in blue is the sensitivity and the second bar in red the positive prediction value.

belong to the LAA. These quantities can be calculated with the following formulas:

$$\text{Sensitivity} = \frac{\text{TP}}{\text{TP} + \text{FN}}; \text{PPV} = \frac{\text{TP}}{\text{TP} + \text{FP}} \tag{4}$$

with TP: True Positive, FP: False Positive, FN: False Negative

We experimentally found that the mesh has some difficulties to reach the tip of the LAA, as illustrated by the sometimes low sensitivity shown on Fig. 4 ; but there are very few segmentation errors, with a good adaptation to the shape of the LAA, as described by the high PPV.

We can observe one major failure with both low sensitivity and PPV (subject 14), and three subjects (2,3,4) with a sensitivity smaller than 60 %. These problems are mainly due to small inaccuracies during the four first segmentation phases occurring near the base of the LAA. The manual segmentation has been able to uphold this problem - apart from the voxels in the base of the LAA - but the automatic segmentation has inflated the mesh in wrong directions, from the beginning. The loop reparation couldn't make the mesh to go in the correct direction, and nearly stopped the algorithm: we preferred to have a small, not very inflated mesh near the base than a twisted mesh anywhere. This undersegmentation of the LAA must be known if this algorithm is used in clinical application. It has been chosen as a compromise between sensitivity and reliability.

5. CONCLUSION

We presented a method combining two types of deformable models integrated in a common framework. This approach enables the segmentation of structures with well defined shapes using shape-constrained deformable models while also enabling the flexible inflation of a high resolution mesh into structures with less predictable shapes. We applied this framework to the segmentation of the left atrial appendage. This combination of deformable models could be applied to other complex anatomical structures.

6. ACKNOWLEDGEMENTS

The research leading to these results has received funding from the European Community's Seventh Framework Programme (FP7/2007-2013) under grant agreement n. 224495 (euHeart project). We would like to thank H. Lehmann and R. Kneser from Philips Research Europe–Aachen for their support. In addition, we thank P. Cignoni and his team for creating the MeshLab software. Finally, we thank H. Delingette for creating the connection between us.

7. REFERENCES

[1] A. F. Frangi, W. J. Niessen, and M. A. Viergever, "Three-dimensional modeling of functional analysis of cardiac images: A review," *IEEE Transactions on Medical Imaging*, vol. 20, no. 1, pp. 2–25, 2001.

[2] O. Ecabert, J. Peters, and H. Schramm et al., "Automatic Model-Based segmentation of the heart in CT images," *IEEE Transactions on Medical Imaging*, vol. 27, no. 9, pp. 1189–1201, September 2008.

[3] Y. Zheng, A. Barbu, and B. Georgescu et al., "Four-chamber heart modeling and automatic segmentation for 3d cardiac CT volumes using marginal space learning and steerable features," *IEEE Transactions on Medical Imaging*, 2008.

[4] J. Lötjönen, S. Kivistö, and J. Koikkalainen et al., "Statistical shape model of atria and ventricles and epicardium from short- and long-axis MR images," *Med. Image Analysis*, vol. 8, pp. 371–286, 2004.

[5] H. C. van Assen, M. G. Danilouchkine, and A. F. Frangi et al., "SPASM: A 3D-ASM for segmentation of sparse and arbitrarily oriented cardiac MRI data," *Medical Image Analysis*, vol. 10, pp. 286–303, 2006.

[6] J.P. Veinot, P.J. Harrity, and F. Gentile et al., "Anatomy of the normal left atrial appendage: a quantitative study of age-related changes in 500 autopsy hearts: implications for echocardiographic examination," *Circ. 96*, vol. 9, pp. 3112–3115, 1997.

[7] C. Stöllberger, B. Schneider, and J. Finsterer, "Elimination of the left atrial appendage to prevent stroke or embolism?," *Chest 124*, vol. 6, pp. 2356–2362, dec 2003.

[8] P. Guigue and O. Devillers, "Fast and robust triangle-triangle overlap test using orientation predicates," *Journal of graphics, gpu, and game tools*, vol. 8, no. 1, pp. 25–42, 2003.